PERGAMON

International Journal of Solids and Structures 38 (2001) 7919–7944

INTERNATIONAL JOURNAL OF SOLIDS and STRUCTURES

www.elsevier.com/locate/ijsolstr

Experimental and numerical study on bending collapse of aluminum foam-filled hat profiles

Weigang Chen *

Impact and Crashworthiness Laboratory, Massachusetts Institute of Technology, Room 5-218, Cambridge, MA 02139, USA

Received 11 July 2000; in revised form 20 April 2001

Abstract

The deep bending collapse of thin-walled empty and foam-filled hat profiles are studied experimentally and numerically. The deep bending tests involve two steps. First, the bending tests are run in a conventional three-point bending mode up to approximately 40° rotation. Then, the bent specimens are loaded vertically in compression, and are bent further up to 150°. These tests revealed salient features of empty and foam-filled hat members subjected to large bending rotations. The moment–rotation characteristics of the generalized plastic hinges with the rotation angle up to 150° are obtained experimentally, and they are found to be qualitatively similar to the case of axial folding of thin-walled members, with peaks and troughs on M–θ curves corresponding respectively to the initiation of foldings and jammings. It is found that foam-filled members provided a 30–40% increase, compared to traditional non-filled members, of the specific energy absorption. Numerical study using explicit nonlinear finite element method are also conducted. Quasi-static simulations of deep bending collapse of empty and foam-filled single-hat beams are carried out. Numerical results are compared with the experimental results showing good agreement.

Keywords: Bending collapse; Empty profiles; Filled profiles; Aluminum foam

1. Introduction

Over the past twenty years, academic institutions and industry have made enormous efforts to understand the mechanisms of structural collapse of thin-walled members in axial folding, and to design efficient energy absorbing members. However, the truth is that axial progressive folding is easily reproducible only in laboratory experiments, and it seldom acts alone in a real crash event. A study on 81 real world vehicle crashes (Kallina et al., 1994) showed that up to 90% involved structural members failed in bending collapse mode.

A first comprehensive study of the bending collapse of prismatic members was made by Kecman (1983). The bending collapse behavior of rectangular and square section was studied theoretically and

* Tel.: +1-734-844-8606.

E-mail address: wgchen@alum.mit.edu (W. Chen).

0020-7683/01/$ - see front matter
PII: S0020-7683(01)00094-4

experimentally. Simple failure mechanisms involving stationary and moving plastic hinge lines were proposed in his analysis, and the moment–rotation characteristics was calculated in the post-failure range up to 40°. A similar approach was developed independently by Abramowicz (1983). Mahmood et al. (1988) developed a bending collapse model which divides the thin-walled cross-section into a number of strips. Experiments for aluminum hat sections undergoing cantilever bending up to 20° were reported by McGregor et al. (1993). Wierzbicki et al. (1994) extended the concept of superfolding element, developed originally for axially loaded columns (Wierzbicki and Abramowicz, 1983; Abramowicz and Wierbicki, 1989), to the case of bending and combined bending/compression loading. Closed-form solutions were derived for the moment–rotation characteristics in the deep bending collapse range.

In order to achieve high weight efficiency in energy absorption, the concept of introducing an ultralight metal filler, such as aluminum foam or aluminum honeycomb, into the thin-walled hollow structural members has received increasing interest. Extensive studies have been carried out by a number of authors on the crushing behavior of axially compressed foam-filled columns (e.g. Seitzberger et al., 2000; Hanssen et al., 1999, 2000a,b; Santosa and Wierzbicki, 1998, Santosa et al., 2000b, Seitzberger and Willminger, 2000). Seitzberger et al. (1997, 2000) conducted experimental studies on the axial crushing of steel columns filled with aluminum foam. Various cross-sections were considered in their studies, including square, hexagonal, octagonal and bitubal arrangements of these cross-sections (two concentrically oriented profiles with aluminum foam in between). Numerical simulation was also carried out using ABAQUS explicit code (Seitzberger et al., 1997). They reported that considerable mass efficiency improvements with respect to energy absorption were obtained by foam filling, particularly the bitubal arrangements. Comprehensive experimental studies on the effect of filling thin-walled square and circular aluminum extrusions with aluminum foam was conducted by Hassen and his colleagues (Hanssen et al., 1999, 2000a,b). Santosa and Wierzbicki (1998) and Santosa et al. (2000b) conducted numerical investigations on the effect of foam filling undergoing axial crushing. Aluminum foam filling was found to be preferable to thickening the column wall in terms of specific energy absorption (energy absorption per unit mass). Chen and Wierzbicki (1999) and Chen and Nardini (2000) carried out experimental studies on crushing behavior of axially compressed sheet aluminum foam-filled sections. Some preliminary results of three-point bending tests up to 40° were also presented in the paper.

Usually, bending collapse of thin-walled members is localized at plastic hinges, with remaining parts of beam-columns rotating as rigid bodies. Only a small portion of the structure is involved in plastic deformation. The plastic bending resistance drops significantly after local sectional collapse occurs at relatively small rotation angle, which results in a low energy absorption efficiency. Santosa et al. (1999) and Santosa et al. (2000a) studied the effect of foam filling on the bending crush resistance of thin-walled steel beam through quasi-static numerical simulations and physical experiments. It was found that the presence of the foam filler offers additional support from inside and suppresses the sectional collapse at the compressive flange, and therefore improves the load carrying capacity, thus maximizes the energy absorption. Chen et al. (2000) conducted optimization study for minimum weight on foam-filled and honeycomb-filled sections undergoing bending collapse and combined bending/compression crushing. The results showed a promising future of thin-walled members with ultralight filler as weight-efficient crash energy absorbers.

In the above mentioned studies, the bending angles of the collapsed beams are limited to 20–30°. However, in a real crash event such as a car crash, this may be well exceeded. The objective of the present work is to study the crushing behavior of aluminum foam-filled hat profiles undergoing very deep bending collapse. Quasi-static bending tests are carried out on empty and foam-filled single and double hat sections. Because the bending angle of a specimen on a conventional three-point bending fixture is usually limited by the depth of the fixture, a new experimental approach is applied so that the specimen can undergo large bending angles up to 150°. In such an approach, the tests are conducted by two steps. First, bending tests are run on a three-point bending fixture up to 40° rotation. Then, the bent specimens are loaded vertically in compression, and they are bent further up to 150°. Some interesting features of the deep bending be-

havior of empty and filled hat members are revealed, and the strengthening effect of foam filling is quantified by the test results.

The finite element simulation on the deep bending of empty and foam-filled single-hat sections are also conducted using non-linear explicit code PAM-CRASH. Simulations are run in two steps similar to those in the experiment by utilizing time sensors. A simple maximum principal stress yielding model is used for aluminum foam in the analysis. Numerical results are compared with the testing results showing good agreement.

2. Experimental study

Quasi-static deep bending tests were conducted on empty and foam-filled hat sections. Three different sections were considered in the present study, which are single-hat, double-hat, and double-hat with closure. The specimens were manufactured at Alcan International, Banbury Laboratory, England. The bending tests were carried out on a 200 kN MTS long stroke universal testing machine at Impact and Crashworthiness Laboratory at the Massachusetts Institute of Technology.

2.1. Specimen preparation

An open-hat section of 50 mm × 50 mm, 2.0 mm gauge and 21 mm flange (Fig. 1) was used as a "standard" section to assemble with closing plate or center plate to form three different types of closed hat sections.

The aluminum foam core was fitted into the open channel before the assemblage by carefully machining. The foam-filled hat members were then assembled with closing plates by spot-welding of 25 mm pitch. The sectional geometries of the finished specimens are illustrated in Fig. 2. The length of specimens is 675 mm.

2.2. Material properties

The aluminum sheet used in the tests is HS5754 (a high strength variant of AA5754). Fig. 3 shows typical uniaxial tensile stress–strain curves of this alloy, obtained from specimen cut from longitudinal, 45-degree and transverse directions.

The aluminum foam (Al–SiC) used in the tests was manufactured and provided by CYMAT Corp. The apparent density of the foam is 0.27 g/cm^3 (measured under atmospheric pressure). Fig. 4 shows the typical stress–strain curves obtained from quasi-static uniaxial compression tests on aluminum foam cubes in three different directions. The directions are defined as: *l*: longitudinal direction of the foam panel; *t*: thickness

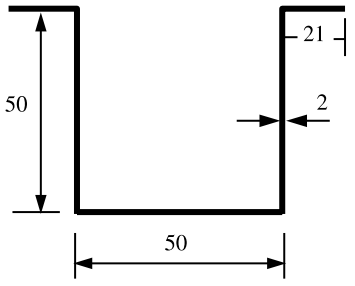

Fig. 1. A "standard" open hat section used in manufacturing specimens.

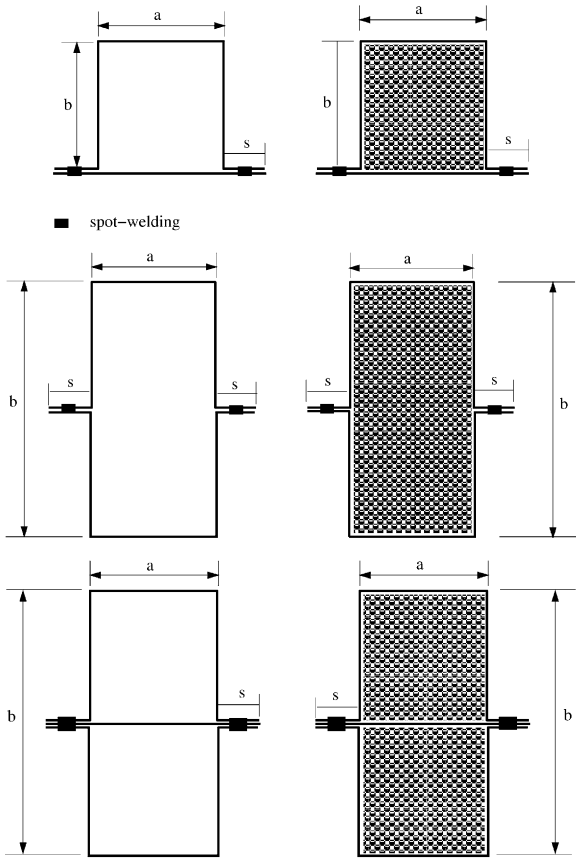

Fig. 2. Sectional geometries of hat sections. First row: single-hat; second row: double-hat; third row: double-hat with closure.

direction of the foam panel; *w*: width direction of the foam panel. As can be seen, the foam shows certain orthotropy, which is associated with its manufacturing process. The foam core is fitted into the hat member with its *l* direction aligning with the longitudinal direction of the beam and its *t* direction aligning with the width direction of the beam.

2.3. Experimental design

The bending tests involve two stages. First, the tests were run on a conventional three-point bending configuration, see Fig. 5(a). The maximum punch displacement was set to be 99 mm (the maximum travel distance available on the three-point bending fixture). The corresponding bending rotation angle is 30–40°, depending on the section type. The specimens were unloaded at the end of the first stage. Subsequently, the bent specimens were loaded vertically in compression for further bending, see Fig. 5(b).

A special end fixture was designed for installing the bent specimens vertically on the testing machine in such a way that one end of the specimen is pin–pin connected with the stroke with two degrees of freedom (vertical displacement and in-plane rotation), and the other end is pin–pin connected with the base of the testing machine with only one in-plane rotational degree of freedom. Fig. 5 shows one such end fixture.

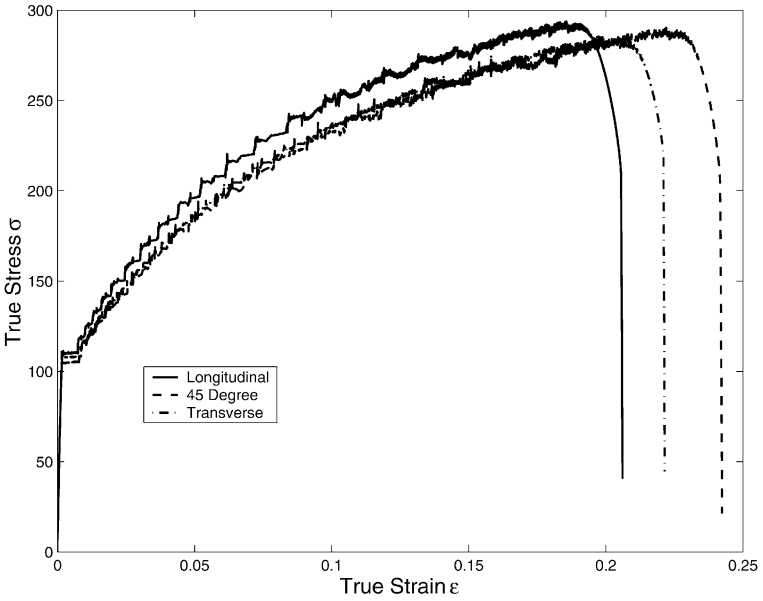

Fig. 3. Stress–strain curves of aluminum alloy HS5754.

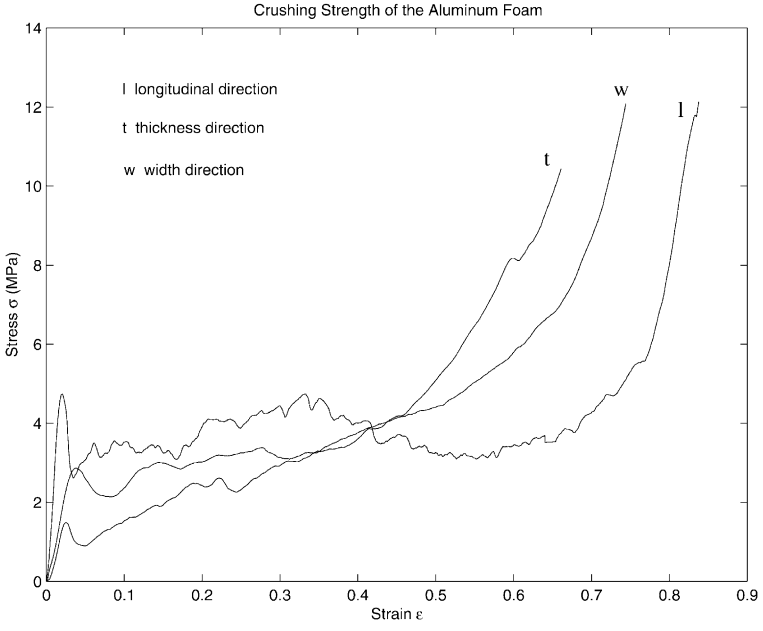

Fig. 4. Stress–strain curves of CYMAT Al–SiC 0.27 g/cm^3 foam.

Via such connection, only forces are transmitted to the ends of specimens, and specimens are bent further up to 150° by compressing the upper end down. All tests were run quasi-statically with a cross-head

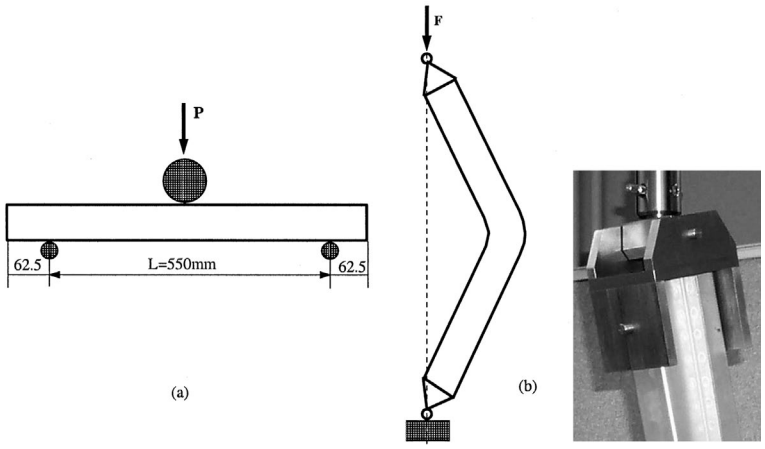

Fig. 5. Experimental setup for the deep bending tests. (a) Stage 1; (b) stage 2.

displacement rate 0.4 mm/s. The vertical force and displacement were recorded at a frequency of 10 Hz in both bending stages.

2.4. Stage I: three-point bending

Three-point bending tests were conducted on 12 specimens. The diameter of the punch was set to be 100 mm (from our experience, a punch with the diameter comparable to the dimension of the cross-section of the specimen is a reasonable choice). The span of the beam between two supporting points was 550 mm. The punch went down with a constant low rate of 0.2 mm/s. The details of specimens are listed in Table 1. The following component test numbering system was applied, e.g. sgl_b1 means the following: sgl: single-hat (dbl for double-hat and dblc for double-hat with closure); b: empty section under bending (bf for foam-filled section under bending); 1: repetition number.

Table 1
The summary of specimens (SH = single-hat; DH = double-hat; DHC = double-hat with closure. Parameters a, b, s are referred to Fig. 2)

Specimen ID	Section type	a (mm)	b (mm)	s (mm)	Foam-filling	Punch travel (mm)
sgl_b1	SH	51.5	54	21.3	Empty	99
sgl_bf1	SH	53	53	20.5	Filled	99
sgl_bf2	SH	53	53.5	20.5	Filled	99
sgl_bf4	SH	53	53.5	20.5	Filled	99
dbl_b1	DH	51	104	20.5	Empty	99
dbl_bf1	DH	53	102.5	21.0	Filled	99
dbl_bf2	DH	52	103	20.5	Filled	99
dbl_bf3	DH	52.5	102.5	20.8	Filled	99
dblc_b1	DHC	51.5	105	20.8	Empty	99
dblc_bf1	DHC	52.5	105	20.8	Filled	99
dblc_bf2	DHC	52	105	20.5	Filled	99
dblc_bf3	DHC	53	104.5	20.5	Filled	99

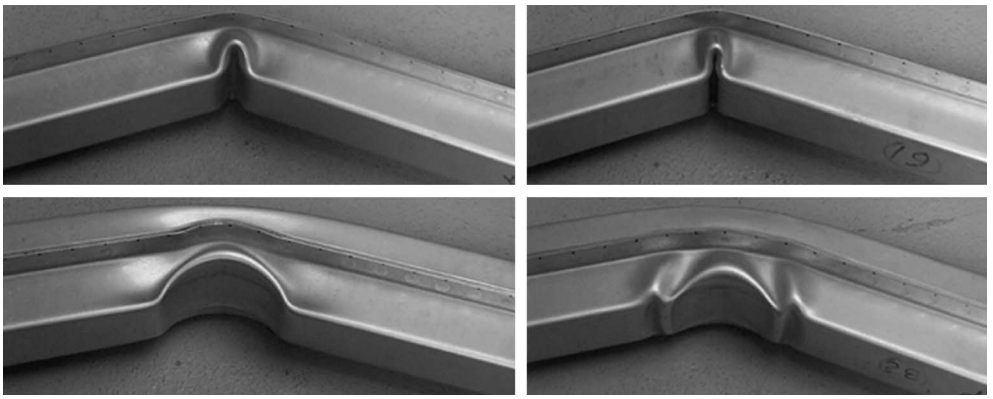

Fig. 6. The deformation patterns of single-hat beams after three-point bending (first row left: empty single-hat; first row right: filled single-hat; second row left: empty double-hat; second row right: filled double-hat).

Some general observations can be made regarding the deformation patterns of both empty and foam-filled beams.

- No joint failure was observed at all the specimens tested, empty or foam-filled;
- One single inward fold was developed at the compression flange and two outward folds at the adjacent sides on single hat beams, both empty and foam-filled ones, see Fig. 6;
- One large inward fold was developed on an empty double-hat beam. The shape of the fold more or less conforms that of the punch. It indicates that the crushing behavior is a combination of a localized indentation (influenced by the shape and size of the punch) and a global bending collapse. In contrast, the inward folding deformation of foam-filled double-hat beam was suppressed by the lateral support of the foam, which resulted in higher bending resistance. The localized folding propagates to the adjacent sections, and more plastic hinge lines were formed, see Fig. 6;
- The deformation patterns of double-hat with closure beams are similar to their double-hat counterparts.

The punch force–displacement curves of single-hat, double-hat and double-hat with closure sections are shown in Figs. 7–9, respectively. As can be seen, the punch forces, and thus the bending resistances are increased due to the foam filling.

2.5. Stage II: vertical compression

The second stage of the deep bending tests was conducted on the bent pieces of the first stage. After unloaded from the three-point bending mode, the bent specimens had small spring-back, which changed the rotation angle by about 1°. They were then vertically mounted and loaded in compression, as shown in Fig. 10. Lengths R and e were measured before compressive loading, and are listed in Table 2.

In this stage, the specimens were bent by being compressed at the ends. The plastic deformation concentrated on the center portion of the beam-column. For simplicity in analysis, the plastic zone at the center portion of the beam-column (see Fig. 10a) was treated as a generalized plastic hinge (see Fig. 10b). The remaining parts of the beam-column were kept undeformed and rotated as rigid bodies.

The compressive force F and the vertical displacement Δ recorded in the quasi-static tests for single-hat, double-hat and double-hat with closure beams are shown in Figs. 11–13, respectively.

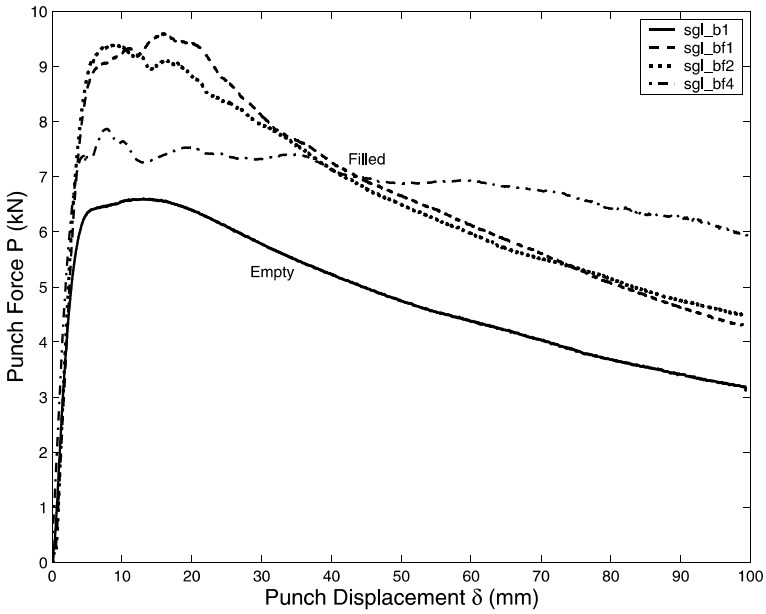

Fig. 7. The punch force–displacement curves of single-hat beams. The specimen IDs sgl_b1, sgl_bf1, sgl_bf2, sgl_bf4 are referred to Table 1.

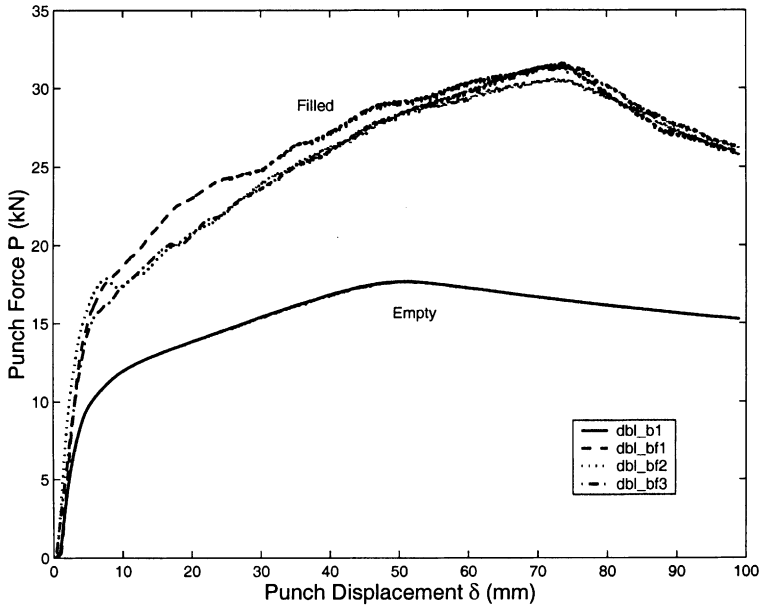

Fig. 8. The punch force–displacement curves of double-hat beams. The specimen IDs dbl_b1, dbl_bf1, dbl_bf2, dbl_bf3 are referred to Table 1.

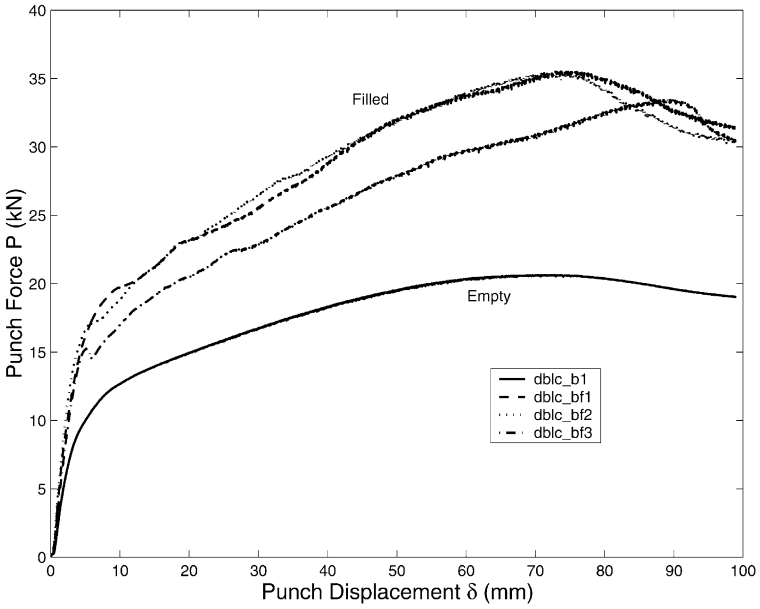

Fig. 9. The punch force–displacement curves of double-hat with closure beams. The specimen IDs dblc_b1, dblc_bf1, dblc_bf2, dblc_bf3 are referred to Table 1.

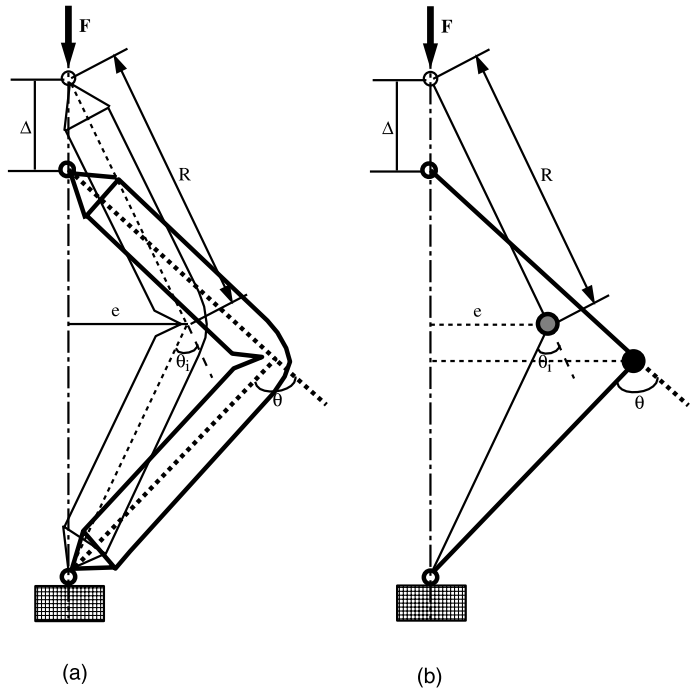

Fig. 10. Vertical compression configuration for the second bending stage.

Table 2
The summary of specimens in the bending stage II (SH = single-hat; DH = double-hat; DHC = double-hat with closure; E = empty; F = filled). Parameters R, e, θ_i, Δ and θ are referred to Fig. 10

Specimen ID	Section type	R (mm)	e (mm)	θ_i (deg)	Δ (mm)	θ (deg)	Fracture
sgl_b1	SH,E	380.5	125	38.4	580	156	No
sgl_bf1	SH,F	380.5	138	42.5	550	153	No
sgl_bf2	SH,F	380.5	136	41.9	502	146	No
sgl_bf4	SH,F	380.5	136	41.9	546	151	No
dbl_b1	DH,E	380.5	95	28.9	548	151	No
dbl_bf1	DH,F	380.5	120	36.8	448	135	No
dbl_bf2	DH,F	380.5	118	36.1	550	152	No
dbl_bf3	DH,F	380.5	115	35.2	51	52	Yes
dblc_b1	DHC,E	380.5	95	28.9	549	151	No
dblc_bf1	DHC,F	380.5	111	33.9	39	48	Yes
dblc_bf2	DHC,F	380.5	112	34.2	46	50	Yes
dblc_bf3	DHC,F	380.5	110	33.6	529	149	No

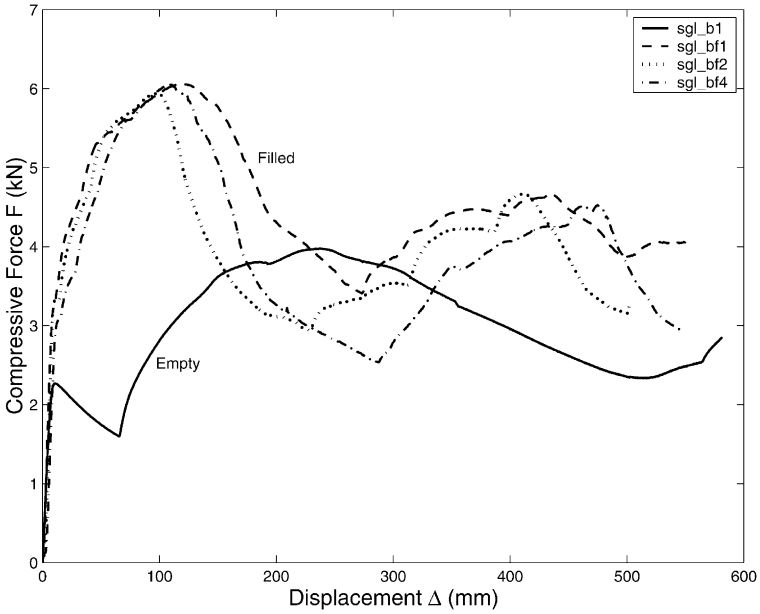

Fig. 11. Compressive force–displacement responses of single-hat beams. The specimen IDs sgl_b1, sgl_bf1, sgl_bf2, sgl_bf4 are referred to Table 2.

A few general observations can be made regarding the bending deformation of various sections.

2.5.1. Single-hat sections

- For the empty single-hat section, the inward folding at the generalized plastic hinge continued at the beginning associated with decreasing of the compressive force, until the first jamming (touching of two sides of the fold, see Fig. 14). At that point, the compressive force started to increase and reached one peak (Fig. 11 empty) when a second fold developed (Fig. 14), and the force dropped accordingly.

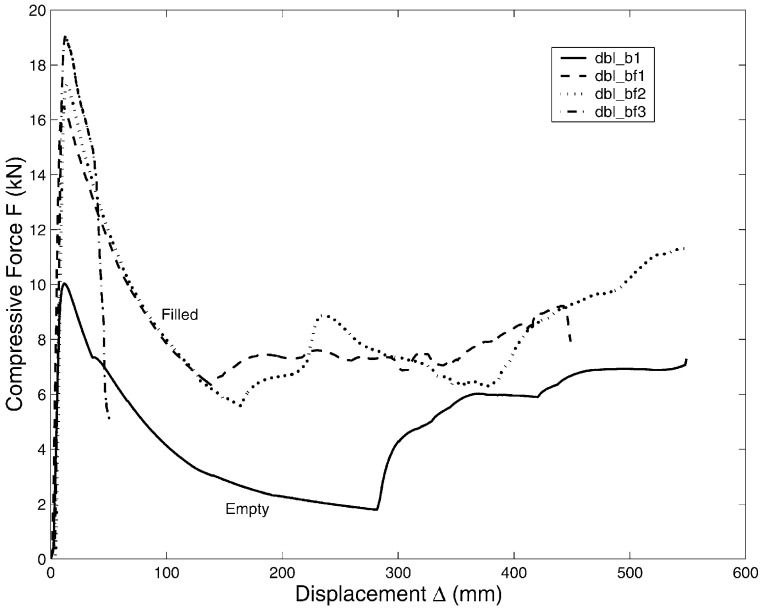

Fig. 12. Compressive force–displacement responses of double-hat beams. The specimen IDs dbl_b1, dbl_bf1, dbl_bf2, dbl_bf3 are referred to Table 2.

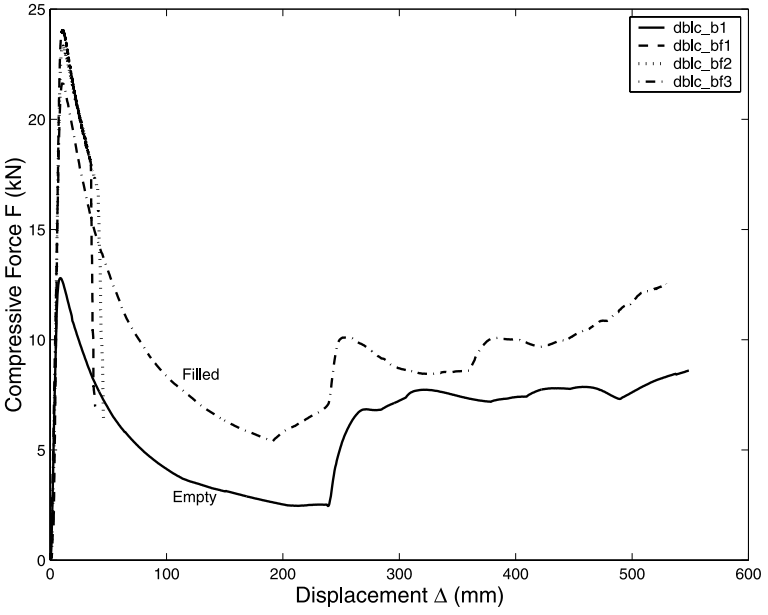

Fig. 13. Compressive force–displacement responses of double-hat with closure. The specimen IDs dblc_b1, dblc_bf1, dblc_bf2, dblc_bf3 are referred to Table 2.

A second jamming started to develop at a large compression (thus large bending rotation), and the force increased again.

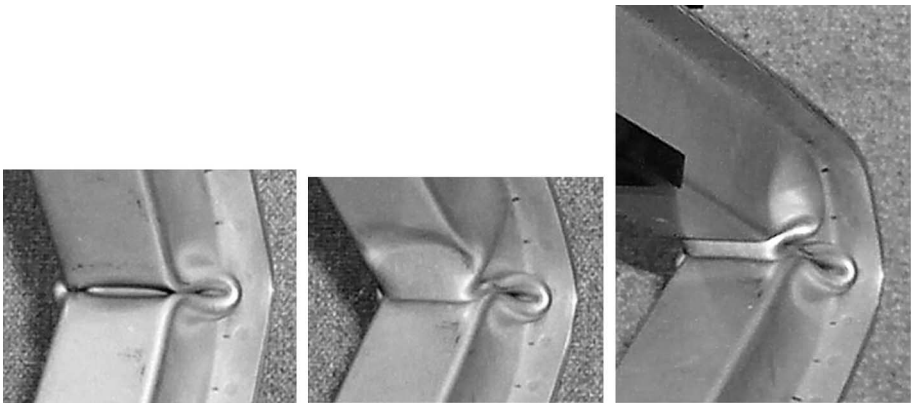

Fig. 14. Bending deformations of empty single-hat beam (from left to right: first jamming, second fold, second jamming).

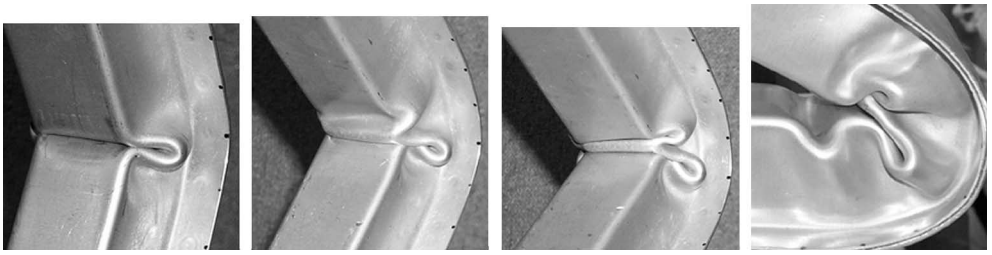

Fig. 15. Bending deformations of filled single-hat beam (from left to right: first jamming, second fold, second jamming, third fold).

- For the foam-filled single-hat beam, the jamming of the first fold developed in the three-point bending stage occurred at the beginning of this bending stage (Fig. 15), and accordingly the compressive force started to climb up to a peak (Fig. 11, filled), where a second fold started (Fig. 15). As a consequence, the force dropped until a second jamming occurred (Fig. 15). At that time the force reached a second peak. After that, a third fold developed and force decreased again.
- The final deformed empty and filled single-hat beams are shown in Fig. 16. Fig. 17 shows a cut-through view of the generalized plastic hinge of two specimens. As can be noted, the foam provided the lateral

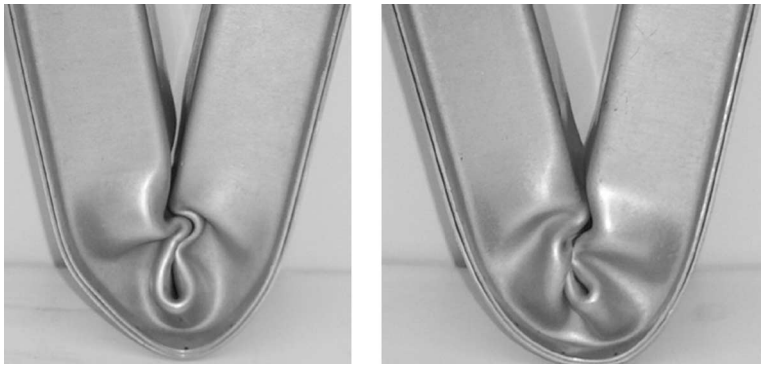

Fig. 16. Bending deformations of empty and filled single-hat beams (left: empty; right: filled).

Fig. 17. Cut-through view of empty and filled single-hat beams (left: empty; right: filled).

support to the compressive flange of the beam, and therefore suppressed the sectional collapse deformation. Three folds were formed at the filled beam, while only two at the empty one. It can also be seen that the foam was subjected to bi-axial loading, with the compression in lateral direction being the dominant component. No appreciable fracture is observed in foam material.

2.5.2. Double-hat section

- For the empty double-hat beam, the large inward fold developed in the bending stage I continued to grow in this stage (Fig. 18), and the compressive force dropped rapidly (Fig. 12, empty) until the jamming developed (Fig. 18). After the jamming, the force increased, which indicates the increasing of the bending moment at the generalized plastic hinge.
- Similarly, the large inward fold on the filled double-hat beam continued to grow at the beginning of this bending stage (Fig. 19), and the compressive force correspondingly dropped rapidly (Fig. 12, filled), until the jamming occurred (Fig. 19). From that point on, the force increased generally, with small fluctuations resulting from small second and third folding and corresponding jammings (Fig. 19).

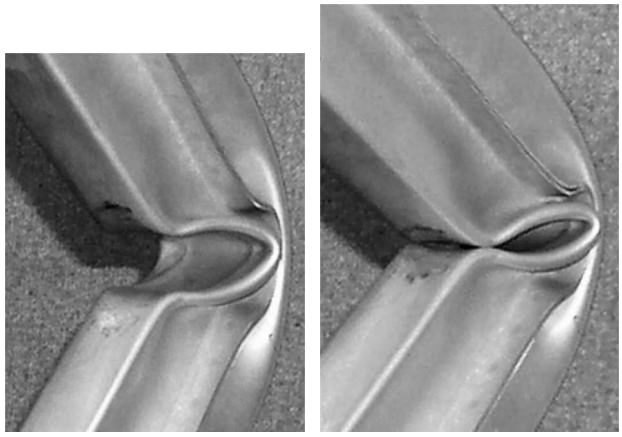

Fig. 18. Bending deformations of empty double-hat beams (left: first fold; right: jamming).

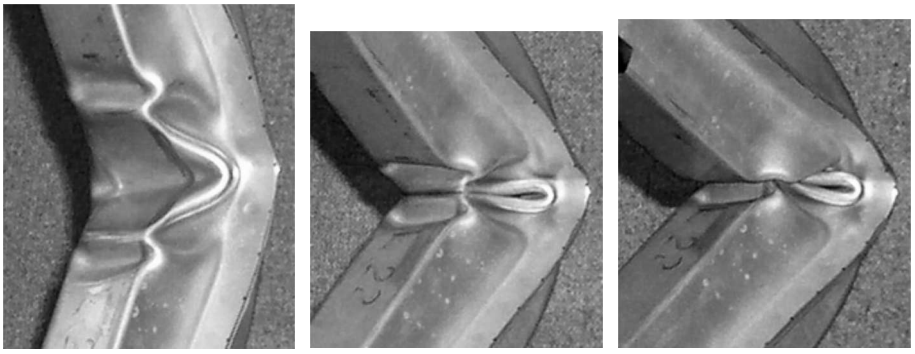

Fig. 19. Bending deformations of filled double-hat beams (left to right: first fold, first jamming, subsequent folds and jammings).

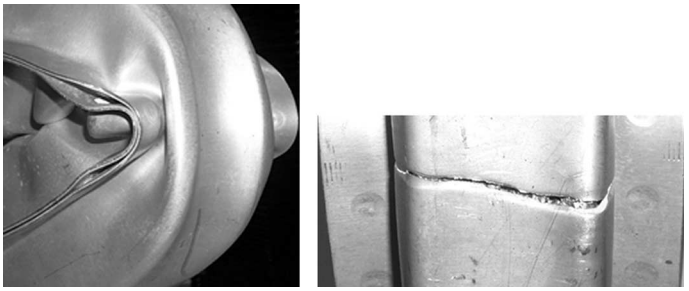

Fig. 20. Negative curvature and fracture at the tensile flange of double-hat beam.

- A negative curvature was developed at the tensile flange of both empty and filled beams (Fig. 20), which relieved the plastic strain and prevented fracture from occurring. One filled beam failed prematurely with fracture at the tensile flange, and the loading capacity diminished consequently (Fig. 12, dbl_bf3).

2.5.3. Double-hat with closure section

- Similar deformation pattern and loading characteristics are observed in empty double-hat with closure beams, as in the case of empty double-hat without closure beams.
- Only one of three filled beams developed large bending rotation, with the deformation characteristics similar to the double-hat counterpart. The other two beams failed prematurely with fracture at the tensile flange. This underlines the importance of the consideration of fracture as a limiting factor of structural strengthening methods, such as foam filling.

2.6. Moment–rotation characteristics

The moment–rotation characteristics of the generalized plastic hinges of various sections can be derived from force-displacement data. From the three-point bending configuration (Fig. 5a), the bending moment and the rotation angle at the plastic hinge in the first bending stage can be calculated approximately from

$$M = \frac{PL}{4}, \tag{1}$$

$$\theta = 2\tan^{-1}\left(\frac{2\delta}{L}\right) \tag{2}$$

where P and δ are punch force and punch displacement in the three-point bending stage, respectively, and L is the beam span.

In the second bending stage (vertical compression), one can idealize the beam-column as a three-hinge mechanism, with the center hinge being the generalized plastic hinge connected with two end hinges via two rigid bars, see Fig. 10(b). The bending moment $M(\theta)$ and bending rotation θ at the plastic hinge can then be approximated as

$$M(\theta) = F \cdot R \sin\frac{\theta}{2} \tag{3}$$

$$\theta = 2\cos^{-1}\left(\cos\frac{\theta_i}{2} - \frac{\Delta}{2R}\right) \tag{4}$$

where F and Δ are the compressive force and vertical displacement, respectively. R is the length of the rigid bar shown in Fig. 10. θ_i is the initial rotation angle at the beginning of the bending stage II.

However, due to the spring-back during the unloading at the end of the bending stage I, the initial angle θ_i is not equal to the final angle θ_0 of the first bending stage. This discrepancy must be taken into account in combining the moment–rotation data of two bending stages into one continuous curve. Accordingly, Eq. (4) should be revised

$$\theta = 2\cos^{-1}\left(\cos\frac{\theta_0}{2} - \frac{\Delta - \Delta_0}{2R}\right) \tag{5}$$

where θ_0 is the final rotation angle of the first stage, and Δ_0 is a displacement correcting shift

$$\Delta_0 = 2R\left(\cos\frac{\theta_i}{2} - \cos\frac{\theta_0}{2}\right). \tag{6}$$

The calculated moment–rotation data in the deep bending range up to 150° rotation angle are plotted in Figs. 21–23, respectively for single-hat, double-hat and double-hat with closure sections. As can be seen, bending moments fluctuate with the bending angle in a way analogous to the axial folding behavior. The peaks and troughs on moment–rotation curves correspond respectively to the formation of subsequent folds and jamming. The bending moments of filled sections are elevated compared to non-filled sections due to the strengthening effect of filling. For those specimens in which fracture developed (dbl_bf3, dblc_bf1, dblc_bf2), the bending moments diminish rapidly.

It is also interesting to note that appreciable drop in bending moment is observed at the transition points of the first bending stage and the second bending stage. The moment drop is partly due to the change of loading condition. In the three-point bending stage, the plastic hinge is subjected to bending moment only (neglecting the shear force). When the first bending stage transits to the second stage, a compressive force acts as well on the plastic hinge in addition to a bending moment.

Assuming that the failure condition of the plastic hinge can be expressed as

$$\left(\frac{M}{M_u}\right) + \left(\frac{N}{N_u}\right) = 1, \tag{7}$$

where M and N are the bending moment and compressive force acting on the plastic hinge at the beginning of the second stage. M_u is the fully plastic bending moment of the section, and can be approximated by the

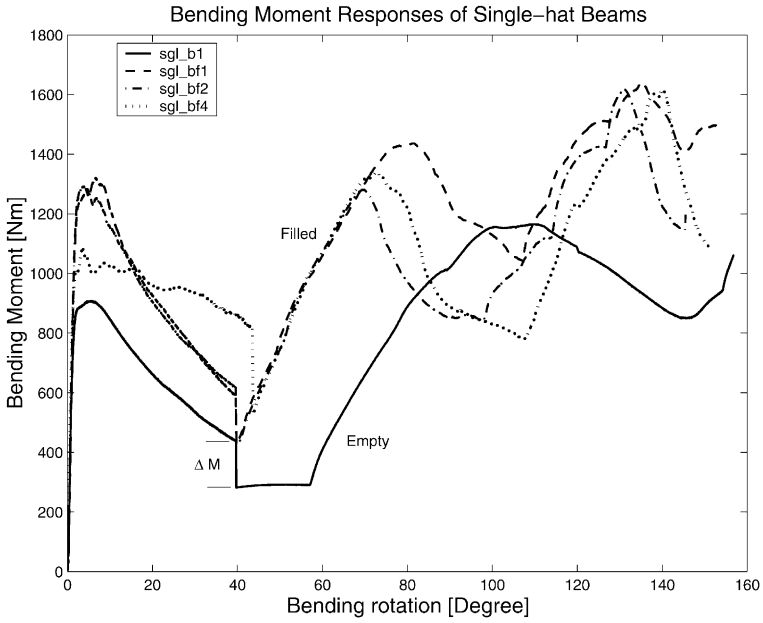

Fig. 21. Moment–rotation responses of single-hat beams. The specimen IDs sgl_b1, sgl_bf1, sgl_bf2, sgl_bf4 are referred to Table 2.

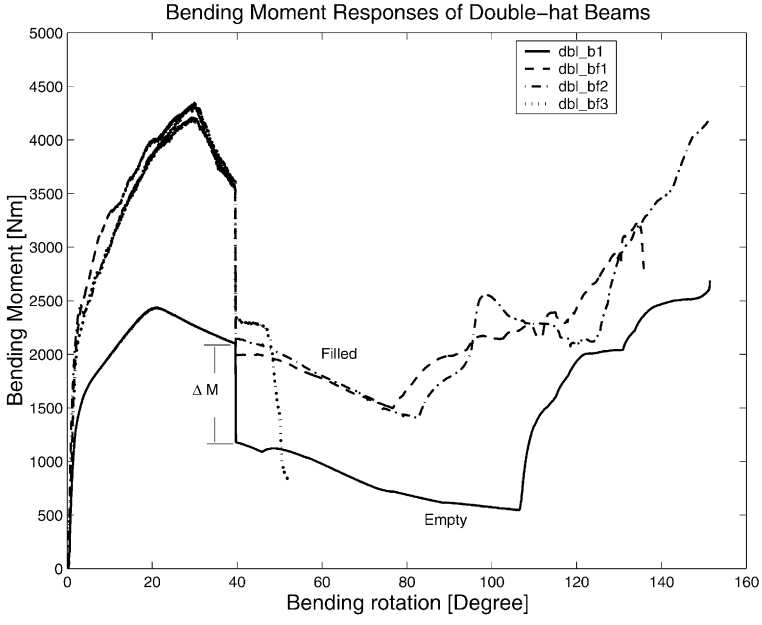

Fig. 22. Moment–rotation responses of double-hat beams (Note a sudden drop in strength of fractured beam dbl_bf3). The specimen IDs dbl_b1, dbl_bf1, dbl_bf2, dbl_bf3 are referred to Table 2.

bending moment developed on the section at the end of the first bending stage. N_u is the squash load of the section, and can be calculated

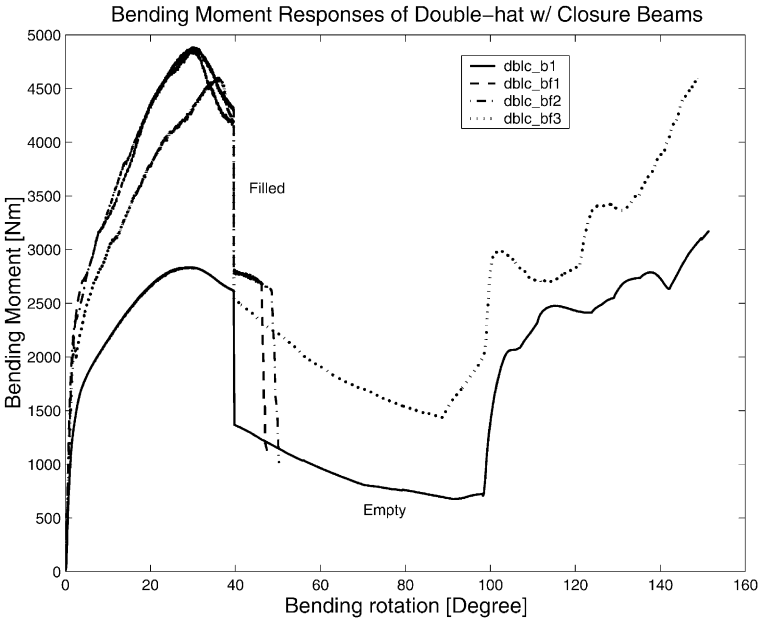

Fig. 23. Moment–rotation responses of double-hat with closure beams (Note a sudden drop in strength of fractured beams dblc_bf1 and dblc_bf2). The specimen IDs dblc_b1, dblc_bf1, dblc_bf2, dblc_bf3 are referred to Table 2.

$$N_u = \sigma_0 A, \tag{8}$$

where σ_0 is the plastic flow stress; A is the sectional area.

Rewriting Eq. (7) leads to the expression for the bending moment M at the beginning of stage II

$$M = \left(1 - \frac{N}{N_u}\right) M_u \tag{9}$$

with

$$N = F \cos\frac{\theta_0}{2} \tag{10}$$

Therefore, the moment drop ΔM can be obtained

$$\Delta M = M_u - M = \frac{N}{N_u} M_u \tag{11}$$

The moment drops predicted by the above equation are listed in Table 3. The experimental results are also shown in the table. One can see that Eq. (11) generally under-predicts the moment drops compared to the experimental results. This could be attributed to several reasons including

(i) the approximate nature of Eq. (7);
(ii) the idealization of three-hinge mechanism;
(iii) the wandering effect of the neutral axis.

Table 3
The moment drop at transition point of two bending stages

Specimen	Moment drop predicted by Eq. (11) (nm)	Moment drop obtained in experiment (nm)
sgl_b1	23	148
sgl_bf1	51	168
sgl_bf2	54	185
sgl_bf4	68	289
dbl_b1	337	922
dbl_bf1	930	1563
dbl_bf2	979	1395
dbl_bf3	1083	1250
dblc_b1	464	1250
dblc_bf1	1400	1487
dblc_bf2	1354	1416
dblc_bf3	1250	1654

2.7. Energy absorption and specific energy absorption

From the moment–rotation data obtained above, the energy E_n absorbed by the specimens during the bending collapse can be calculated from the definition (neglecting the elastic deformation at the very beginning)

$$E_n = \int_0^{\theta_f} M(\theta)\mathrm{d}\theta \tag{12}$$

where θ_f is the final rotation angle.

The specific energy absorption (SEA), which is defined as the energy absorption per unit mass of structural member, can be calculated by

$$\mathrm{SEA} = \frac{E_n}{m_s + m_f} \tag{13}$$

where m_s and m_f are the mass of the sheet metal and the mass of the foam filler, respectively.

Due to the localized nature of the bending collapse, filling beams with foam only at strategic locations, instead of the whole beam length, will still get high bending resistance, while the weight penalty from the filler is greatly reduced and thus the SEA will be much higher. This concept of partial filling was verified experimentally and numerically by Santosa et al. (1999). A simple formula to estimate the effective foam length L_f (see Fig. 24) was proposed by Santosa et al. (1999)

$$L_f = L\left(\frac{\eta - 1}{\eta}\right) - 2H \tag{14}$$

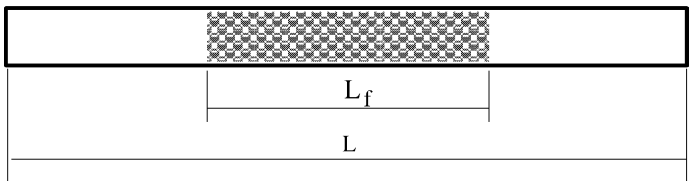

Fig. 24. An illustration of partial filling.

Table 4
Energy absorption and specific energy absorption of specimens ($\theta_f = 150°$)

Specimen	E_n (kJ)	Gain in E_n	Full filling			Partial filling		
			Mass (kg)	SEA (kJ/kg)	Gain in SEA	Mass (kg)	SEA (kJ/kg)	Gain in SEA
sgl_b1	2.048	/	1.043	1.964	/	1.043	1.964	/
sgl_bf1	3.020	47%	1.400	2.157	10%	1.129	2.675	36%
sgl_bf2	2.620	28%	1.400	1.871	−4.7%	1.123	2.333	19%
sgl_bf4	2.767	35%	1.340	2.065	5%	1.075	2.574	31%
dbl_b1	3.920	/	1.407	2.786	/	1.407	2.786	/
dbl_bf1	6.381	63%	2.121	3.808	8%	1.666	3.829	37%
dbl_bf2	6.729	72%	2.121	3.173	14%	1.665	4.038	45%
dbl_bf3[a]	2.804	−2.8%	2.121	1.322	/	/	/	/
dblc_b1	4.795	/	1.750	2.740	/	1.750	2.740	/
dblc_bf1[a]	3.046	−36%	2.464	1.236	/	/	/	/
dblc_bf2[a]	3.165	−34%	2.464	1.284	/	/	/	/
dblc_bf3	7.225	51%	2.464	2.932	7%	1.972	3.663	34%

[a] Failed with premature fracture.

where L is the beam length; η is a scaling parameter, $\eta = M_f/M_0$ with M_f being the ultimate bending moment of filled section and M_0 being the ultimate bending moment of empty section; H is the half folding wave length and can be calculated by

$$H = 1.276 b^{2/3} t^{1/3} \tag{15}$$

where b and t are sectional width and wall thickness, respectively.

The energy absorption and the SEA of specimens with full filling and partial filling are calculated and listed in Table 4. One can see that by partial filling, the SEAs of single-hat and double-hat beams can be increased by around 30% and 40%, respectively, compared to their non-filled counterparts. However, the capacity of energy absorption of some filled double-hat specimens are greatly reduced due to the premature fracture failure. The fracture on filled members should thus be a subject of further research.

It is also worth noting that the gain in SEA will reach around 70% in bending collapse mode with smaller wall thickness and a medium foam density, according to the optimization study (Chen et al., 2000). The parameters of the foam-filled sections must be optimized to achieve the most weight-efficient energy absorption.

3. Numerical study

Numerical simulations are conducted using explicit non-linear finite element code PAM-CRASH on the empty and foam-filled single-hat beams. Similarly as in the physical testing, numerical simulations are modeled as a quasi-static process, and consist of two bending stages: three-point bending (stage I) and a subsequent vertical compression (stage II). Details are discussed in the following.

3.1. Finite element modeling

Thin-walled single-hat beams with sectional geometry shown in Fig. 2 and length 675 mm is considered in the analysis. The outer skin of the beam is modeled with Belytschko–Tsay four-node shell elements. Due to the localized nature of the bending deformation, the central portion where the bending collapse is expected is modeled with fine mesh (2.5×5 mm^2 mesh size). The remaining parts of the beam, which rotate as

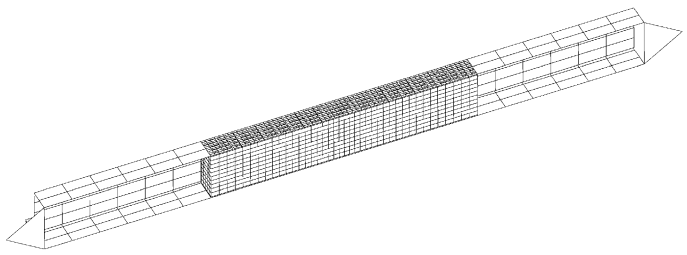

Fig. 25. The finite element model of a single-hat beam.

rigid bodies during bending, are modeled with very coarse mesh to reduce computation time, see Fig. 25. At the interface of fine mesh and coarse mesh, nodes are connected by rigid body mechanisms. The aluminum foam core is modeled with eight-node solid elements. The interaction between the foam core and the skin is simulated by a surface-to-surface sliding contact. Due to the expected symmetry of deformation, only a half of the beam is modeled in the analysis, and symmetry boundary conditions are applied at corresponding plane. Two rigid triangular plates are defined at two ends of the beam to model the end fixture where displacement boundary conditions are applied in the bending stage II.

Two time sensors are defined in the analysis. Sensor I controls the punch and two supports, and sensor II controls the vertical compression process. At the beginning of the simulation, sensor I is activated, and the punch, which is modeled as a moving rigid cylinder with diameter 100 mm, and two supports, which are modeled as stationary rigid cylinders with 550 mm distance between, are active in the model. The velocity boundary condition is applied on the rigid punch with downward speed. When the punch displacement reaches 99 mm, the sensor I is deactivated, and therefore the punch and two supports are removed from the model. Meanwhile, sensor II is activated, which triggers the displacement boundary conditions at two ends of the beam. All DOFs except the in-plane rotation of one end of the beam are fixed, while the other end has two DOFs, longitudinal movement and in-plane rotation. Velocity boundary condition is applied at the moving end. Consequently, the bending stage is transitted smoothly from three-point bending to vertical compression.

3.2. Material modeling

The wall material of the beam is aluminum alloy HS5754, with Young's modulus $E = 70\,\text{GPa}$, initial yield stress $\sigma_y = 108$ MPa, ultimate strength $\sigma_u = 237$ MPa, and Poisson's ratio $v = 0.33$. The constitutive behavior is based on an elastic–plastic material model with Von Mises's isotropic plasticity algorithm with plastic hardening. The plastic hardening data is obtained by averaging three uniaxial tensile tests shown in Fig. 3.

The mechanical behavior of aluminum foam is characterized by elastic modulus E_f, plastic collapse stress σ_f, shear modulus G_f, plastic shear strength τ_f, and densification strain ϵ_D, see Fig. 26. These parameters strongly depend on the aluminum foam density ρ_f.

PAM-CRASH provides a material model for metallic cellular solids such as aluminum foam capable of undergoing large strain deformation. The mechanical properties of cellular solids are described in three orthogonal directions. No interaction among components of the stress tensor is considered in the yield condition of this material model. Thus it is essentially a maximum principal stress yielding model.

The mechanical properties of the aluminum foam used in the experiments (CYMAT Al–SiC foam, 10% relative density) are obtained by calibrating the uniaxial compressive test data shown in Fig. 4. Due to lack of experimental data, the plastic shear strength is taken to be a half of the plastic collapse stress, and the shear modulus G_f is set equal to elastic modulus E_f.

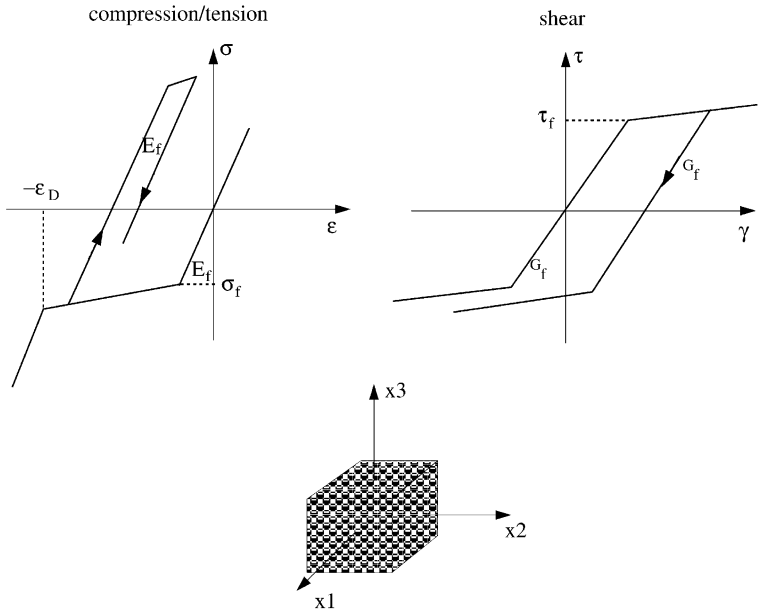

Fig. 26. The material model for aluminum foam.

3.3. Numerical results

The deformation modes of an empty and a foam-filled single-hat beam at the end of the bending stage I are shown in Figs. 27 and 28, respectively. The corresponding post-test specimens are also shown in the same figures. One can see from those figures that the deformation patterns predicted by numerical simulations agree well with the experiments.

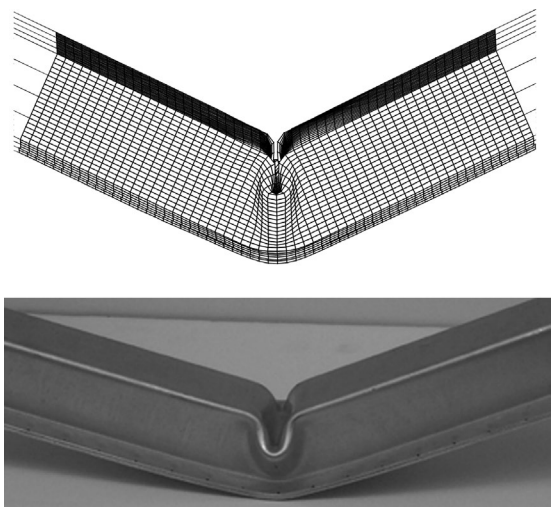

Fig. 27. The deformation modes of empty single-hat beams at the end of bending stage I: numerical and experimental.

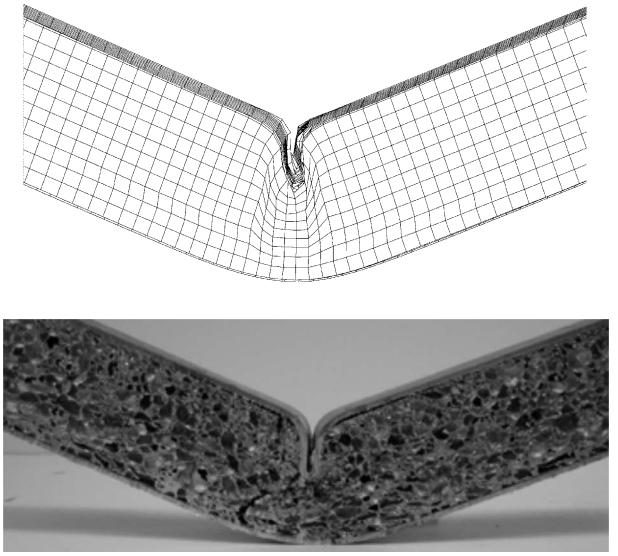

Fig. 28. Cut-through of filled single-hat beams at the end of bending stage I: numerical and experimental.

Figs. 29–31 shown the deformation patterns of empty and filled beams at the end of bending stage II. Post-test specimens are also shown in the same figures for comparison. As can be seen, very good agreement is obtained between numerical simulations and physical testings in the light of bending collapse deformation.

The punch force–displacement responses in stage I and the compressive force–vertical displacement responses in stage II are shown in Figs. 32 and 33, respectively. As can be noted, the numerical results in bending stage I generally show good correlations with experimental results, except that numerical simu-

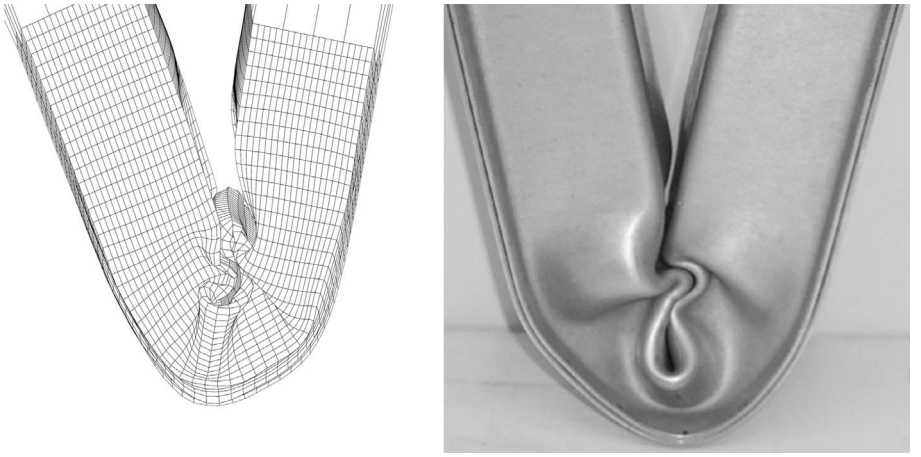

Fig. 29. Bending collapse deformation of empty beams at the end of bending stage II: numerical and experimental.

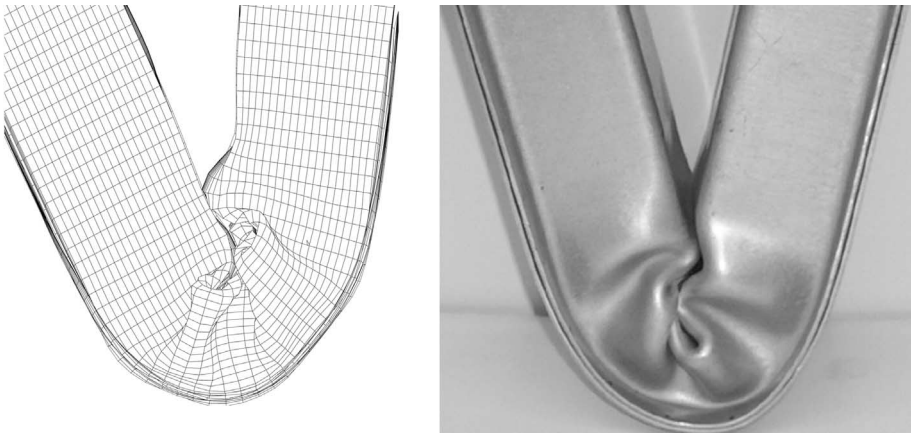

Fig. 30. Bending collapse deformation of filled beams at the end of bending stage II: numerical and experimental.

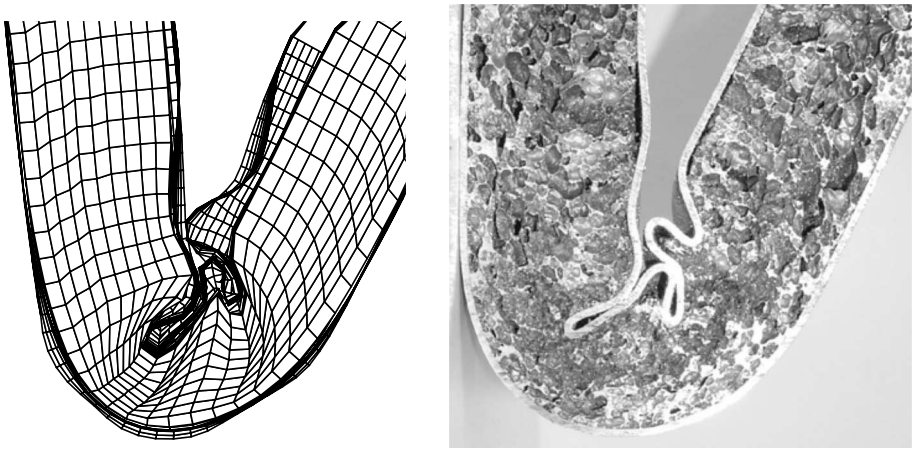

Fig. 31. Cut-through view of filled beams at the end of bending stage II: numerical and experimental.

lations over-predict the peak loads. The reason for this is that finite element model did not capture the initial geometrical imperfections and finite corner radius of sections inherent in real structures.

Two bending stages in numerical simulations are run continuously without unloading. Accordingly, a displacement shift Δ_0, as discussed in the previous section, must be taken into consideration in comparing the numerical and experimental results. One can see that the numerical results and experimental data of both empty and filled beams shown reasonably good agreements in bending stage II.

The above comparisons between the numerical and experimental results validates the finite element modeling technique used in the present work. More numerical analyses are to be carried out with various sectional geometries and foam densities, for the purpose of studying and quantifying the strengthening effect of foam filling in the wide range of material parameters.

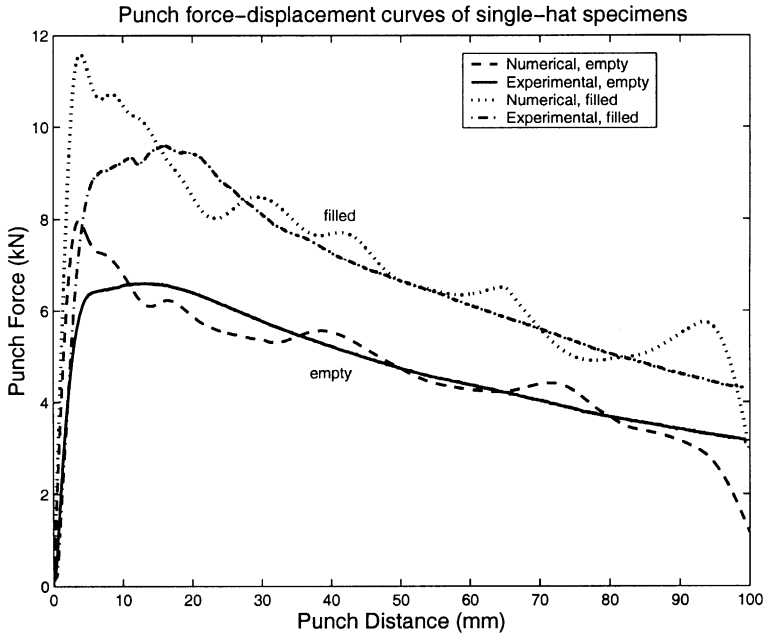

Fig. 32. The punch force–displacement responses of beams in bending stage I.

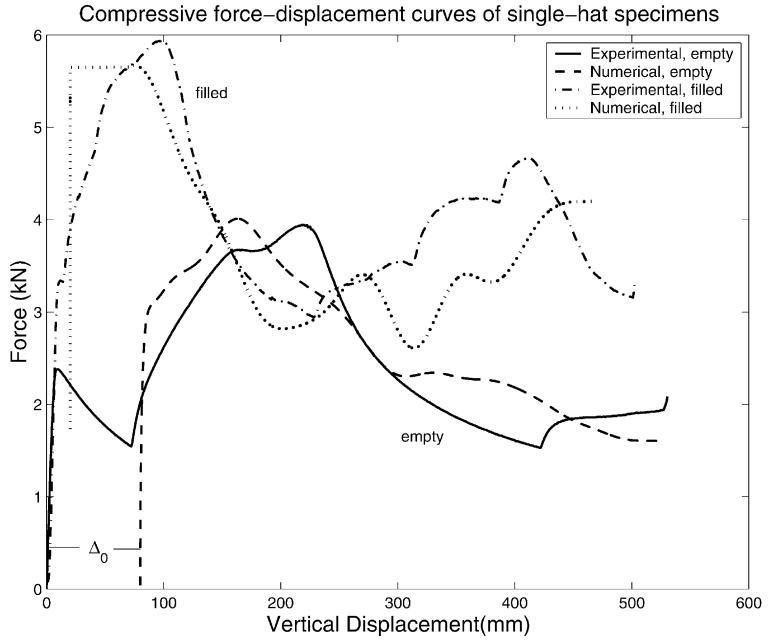

Fig. 33. The compressive force–displacement responses of beams in bending stage II.

4. Concluding remarks

The deep bending collapse of thin-walled empty and foam-filled hat profiles are studied experimentally and numerically in this paper. Three different hat profiles are considered, single-hat, double-hat and double-hat with a closure. A new experimental approach is applied to conduct bending collapse tests with very large rotation angles. The approach involve two steps. First, the beams are deformed in a conventional three-point bending mode up to approximately 40° rotation. Then, the bent specimens are loaded vertically in compression, and are bent further up to 150°.

Some important features of crushing behavior of empty and foam-filled hat members with large bending rotation are revealed, and differences in failure modes among three types of profiles are discussed. The moment–rotation characteristics are obtained experimentally for the generalized plastic hinges with the rotation angle up to 150°, and they are found to be similar to the case of axial folding of thin-walled members, with peaks and troughs on M–θ curves corresponding respectively to the initiation of buckles and formation of subsequent folds all the way to jamming.

It is found in the experimental study that foam-filled members with the current design of sectional geometry and foam density can achieve 30–40% increase in the SEA, compared to traditional non-fill members. This proves great potentials of foam-filled structures as weight-efficient energy absorbers.

Some foam-filled double-hat specimens failed prematurely by developing necking and fractures at tensile flanges, which diminished energy absorption. This underlines the importance of fracture in filled structures as a subject of further research.

Numerical study using explicit nonlinear finite element method is also conducted. Quasi-static simulations of deep bending collapse of empty and foam-filled single-hat beams are carried out. A maximum principle stress yielding model is used for aluminum foam in the analysis. Numerical results are compared with the experimental results showing good agreement, which validates the finite element modeling techniques used in the analysis. More numerical analyses need to be carried out with considerations of various sectional geometries and foam densities, for the purpose of studying and quantifying strengthening effect of foam filling.

Acknowledgements

The present research was conducted for the Project of the "Ultralight" Consortium at MIT. The financial support of all members of the Consortium is gratefully acknowledged. Thanks are due to Altair Computing and Engineering System International for providing free academic licenses of the programs HYPERMESH and PAM-CRASH. The author also wishes to express his appreciation to Dr. Dubravko Nardini, Mr. Jim Tansley at Alcan International Laboratory in England, and Mr. Steve Rudolph at MIT for their assistances in preparing specimens.

References

Abramowicz, W., 1983. Simplified crushing analysis of thin-walled columns and beams. Engineering Transactions 29, 3–27.

Abramowicz, W., Wierbicki, T., 1989. Axial crushing of multicorner sheet metal columns. Journal of Applied Mechanics 56, 113–120.

Chen, W., Nardini, D., 2000. Experimental study of crush behavior of sheet aluminum foam-filled sections. International Journal of Crashworthiness 5 (4).

Chen, W., Wierzbicki, T., 1999. Experimental study on the crushing behavior of aluminum closed-hat foam-filled sections. Impact and Crashworthiness Laboratory, Report no. 26, MIT.

Chen, W., Wierzbicki, T., Santosa, S., 2000. Bending collapse of thin-walled beams with ultralight filler: numerical simulation and weight optimization. Acta Mechanica, in press.

Hanssen, A., Langseth, M., Hopperstad, O., 1999. Static crushing of square aluminum extrusions with aluminum foam filler. International Journal of Mechanical Sciences 41, 967–993.

Hanssen, A., Langseth, M., Hopperstad, O., 2000a. Static and dynamic crushing of circular aluminum extrusions with aluminum foam filler. International Journal of Impact Engineering 24, 475–507.

Hanssen, A., Langseth, M., Hopperstad, O., 2000b. Static and dynamic crushing of square aluminum extrusions with aluminum foam filler. International Journal of Impact Engineering 24, 347–383.

Kallina, I., Zeidler, F., Baumann, K., Scheunest, D., 1994. The offset crash against a deformable barrier, a more realistic frontal impact. Proceedings to the 14th International Technical Conference on Enhanced Safety of Vehicles, Munich, Germany, vol. 2, pp. 1300–1304.

Kecman, D., 1983. Bending collapse of rectangular and square section tubes. International Journal of Mechanical Sciences 25 (9–10), 623–636.

Mahmood, H., Paluszny, A., Lin, Y., 1988. Bending deep collapse of automotive type components. SAE Paper 885044.

McGregor, I., Meadows, D., Scott, C., Seeds, A., 1993. Impact performance of aluminum structures. In: Jones, N., Wierzbicki, T. (Eds.), Structural Crashworthiness and Failure. Elsevier, Amsterdam.

Santosa, S., Banhart, J., Wierzbicki, T., 1999. Bending crush resistance of partially foam-filled sections. Presented at the International Conference on Metal Foams and Porous Metal Structures, Bremen, Germany, 14–16 June.

Santosa, S., Banhart, J., Wierzbicki, T., 2000a. Experimental and numerical analysis of bending of foam-filled sections. Acta Mechanica, in press.

Santosa, S., Wierzbicki, T., 1998. Crash behavior of box column filled with aluminum honeycomb or foam. Computers and Structures 68 (4), 343–368.

Santosa, S., Wierzbicki, T., Hanssen, A., Langseth, M., 2000b. Experimental and numerical studies of foam-filled sections. International Journal of Impact Engineering 24, 509–534.

Seitzberger, M., Rammerstorfer, F., Degischer, H., Gradinger, R., 1997. Crushing of axially compressed steel tubes filled with aluminum foam. Acta Mechanica 125, 93–105.

Seitzberger, M., Rammerstorfer, F., Gradinger, R., Degischer, H., Blaimschein, M., Walch, C., 2000. Experimental studies on the quasti-static axial crushing of steel columns filled with aluminum foam. International Journal of Solids and Structures 37, 4125–4147.

Seitzberger, M., Willminger, S., 2000. Application of plastic collapse mechanisms for the axial crushing analysis of tubular steel structures filled with aluminum foam. In: Chirwa, E.C., Otte, D. (Eds.), Proceedings of ICrash 2000, RAS, Service Point, UK.

Wierzbicki, T., Abramowicz, W., 1983. On the crushing mechanics of thin-walled structures. Journal of Applied Mechanics 50, 727–739.

Wierzbicki, T., Recke, L., Abramowicz, W., Gholami, T., Huang, J., 1994. Stress profiles in thin-walled prismatic columns subjected to crush loading-ii. bending. Computers and Structures 51, 625–641.